IOPscience iopscience.iop.org

Home Search Collections Journals About Contact us My IOPscience

Plasmonic energy transfer in periodically doped graphene

This article has been downloaded from IOPscience. Please scroll down to see the full text article.

2013 New J. Phys. 15 033042

(http://iopscience.iop.org/1367-2630/15/3/033042)

View the table of contents for this issue, or go to the journal homepage for more

Download details:
IP Address: 84.78.211.145
The article was downloaded on 27/03/2013 at 08:35

Please note that terms and conditions apply.

New Journal of Physics
The open access journal for physics

Plasmonic energy transfer in periodically doped graphene

I Silveiro, A Manjavacas, S Thongrattanasiri and F J García de Abajo[1]
IQFR-CSIC, Serrano 119, E-28006 Madrid, Spain
E-mail: J.G.deAbajo@nanophotonics.es

New Journal of Physics **15** (2013) 033042 (11pp)
Received 13 January 2013
Published 26 March 2013
Online at http://www.njp.org/
doi:10.1088/1367-2630/15/3/033042

Abstract. We predict unprecedentedly large values of the energy-transfer rate between an optical emitter and a layer of periodically doped graphene. The transfer exhibits divergences at photon frequencies corresponding to the Van Hove singularities of the plasmonic band structure of the graphene. In particular, we find flat bands associated with regions of vanishing doping charge, which appear in graphene when it is patterned through gates of spatially alternating signs, giving rise to intense transfer rate singularities. Graphene is thus shown to provide a unique platform for fast control of optical energy transfer via fast electrostatic inhomogeneous doping.

Plasmons can interact strongly with light, leading to large electromagnetic field enhancement and concentration of optical energy. These properties have been extensively investigated for applications such as sensing (e.g. via surface-enhanced Raman scattering, down to the single-molecule level [1]), photovoltaics [2], nonlinear optics [3] and catalysis [4]. The presence of plasmons can substantially modify the behavior of optical emitters (e.g. molecules and quantum dots), giving rise to changes in the decay rates [5, 6]. This is quantified through modulations in the local density of optical states (LDOS), which measures the intensity of the normalized

[1] Author to whom any correspondence should be addressed.

Content from this work may be used under the terms of the Creative Commons Attribution 3.0 licence. Any further distribution of this work must maintain attribution to the author(s) and the title of the work, journal citation and DOI.

© IOP Publishing Ltd and Deutsche Physikalische Gesellschaft

photon modes as a function of position and energy [7, 8]. The dipole-like decay rate of an emitter is proportional to the LDOS and can be dramatically boosted by plasmons [9, 10]. A more intuitive picture is suggested by the fact that the energy of a plasmon extends over a region that is small compared with the light wavelength, thus resulting in better matching to the small physical size of the emitter. The energy transferred from an optical emitter to a neighboring plasmon can be either re-radiated (e.g., mediated by confined plasmons) or inelastically absorbed by the plasmonic material (e.g. via coupling to phonons and electron–hole pairs). The balance between these two channels determines whether the plasmon produces enhancement or quenching of the radiative decay relative to free space, depending on the extension of the plasmon and the position of the emitter [11].

In this context, highly doped graphene has emerged as a powerful plasmonic material capable of confining electromagnetic energy down to unprecedented small volumes [12]. The wavelength of graphene plasmons is considerably reduced with respect to the free-space light wavelength, which results in large LDOS values and a significant increase in the interaction with nearby optical emitters compared to conventional plasmonic materials [13]. Additionally, graphene plasmons are tunable through electrostatic doping [14], which suggests a practical way of realizing ultrafast electrical control of both light fields and emission decay rates. The existence and electrical tunability of graphene plasmons have been conclusively demonstrated through direct spatial mapping [15, 16]. In addition to their intrinsic fundamental interest, graphene plasmons are also attracting considerable attention because of their potential application to fast nanoscale light modulation [17], guiding [18] and the control of quantum phenomena [19].

An alternative way of achieving fast decay rates consists in using periodic structures, which lead to divergences in the LDOS associated with the Van Hove singularities [20] of the photonic bands [21]. Periodic plasmon bands in graphene have recently been shown to produce interesting Fano reflection resonances [22] and complete optical absorption [17, 23]. In this paper, we discuss graphene plasmon bands under periodic doping conditions, including the effect of inhomogeneous doping charge distributions. An important conclusion of our work is that the increase in the LDOS near graphene can be made even larger via the Van Hove singularities emerging in the LDOS of the two-dimensional (2D) plasmonic band structure. Our study relies on the analysis of the optical response of graphene under two different types of periodic doping, with either equal-sign or alternating-sign gates, leading to an intricate behavior that we, however, describe via semi-analytical methods in a rigorous manner. The reported results can find applications in infrared sensing and spectral microscopy.

The optical excitations of extended, homogeneously doped graphene can be represented as a function of parallel wave vector $k_{\parallel}$ and energy of the incident light as shown in figure 1(a). Intraband and interband electron–hole pair excitations are shown as the lower and upper shaded areas, respectively. A narrow plasmon band appears in the gap between these regions [14]. Incidentally, the light line is almost indistinguishable from the vertical axis for typical Fermi energies E_F of a few tens of eV [15, 16], so that the optical response can be described electrostatically. When the graphene is periodically doped, we can conveniently project the plasmon band on the first Brillouin zone (see figure 1(b)), where gaps are produced at the zone boundaries, leading to Van Hove singularities in the LDOS. For a sufficiently large period a compared with the graphene Fermi wavelength (e.g., $2\pi/k_F \approx 14\,\text{nm}$ for $E_F = 0.3\,\text{eV}$, and $a \sim 100\,\text{nm}$), these LDOS singularities originate in well-defined plasmons that lie outside the electron–hole pair continuum (figure 1(b)). These are the conditions that we assume in the rest

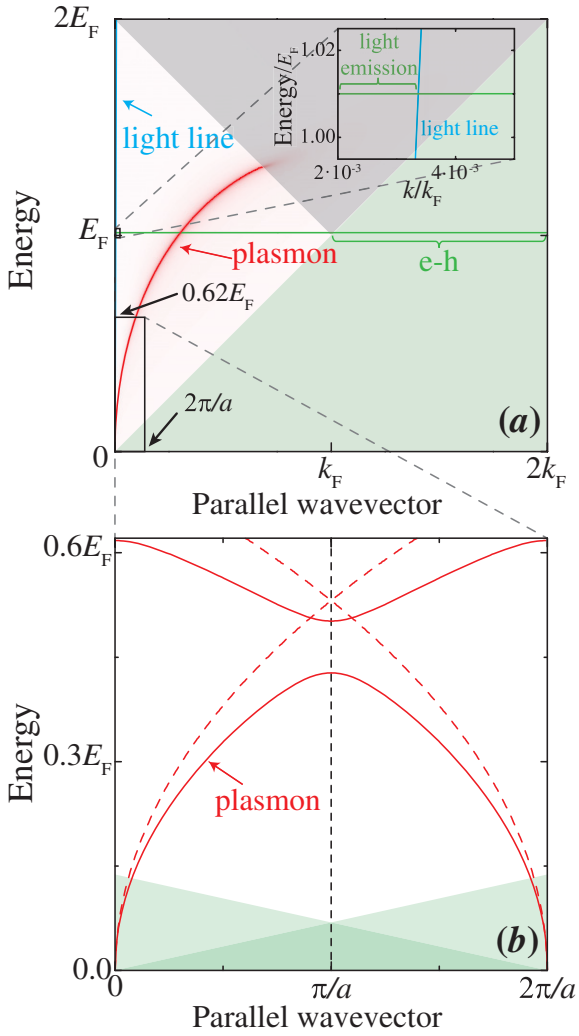

Figure 1. Schematic representation of the contributions to the decay of an optical emitter in front of (a) homogeneously doped graphene and (b) periodically doped graphene. In the periodic structure (b), plasmon bands are first folded over the first Brillouin zone (dashed curves), followed by energy shifts and gap opening.

of the present study. Our results are presented in dimensionless units, so they are applicable to any specific values of the Fermi energy and the lattice period, provided the above conditions are fulfilled.

From a practical point of view, graphene can be periodically doped with nanoscale periods by depositing it on a patterned backgate [18]. Charge transfer from periodically self-assembled atomic species offers another promising alternative [24], particularly for small spacings of just a few nanometers [25]. For convenience, we introduce doping through a square array of periodically arranged external charges of either equal (figure 2(a)) or alternating (figure 2(b)) sign, placed with period a at a distance d from the graphene plane. We describe the graphene using the Drude model for the conductivity [12] $\sigma(\mathbf{R}, \omega) = (\mathrm{i}e^2|E_\mathrm{F}(\mathbf{R})|/\pi\hbar^2)/(\omega + \mathrm{i}\gamma)$, where the Fermi energy E_F varies periodically along the carbon plane, and we assume that $0 < \gamma \ll \omega$.

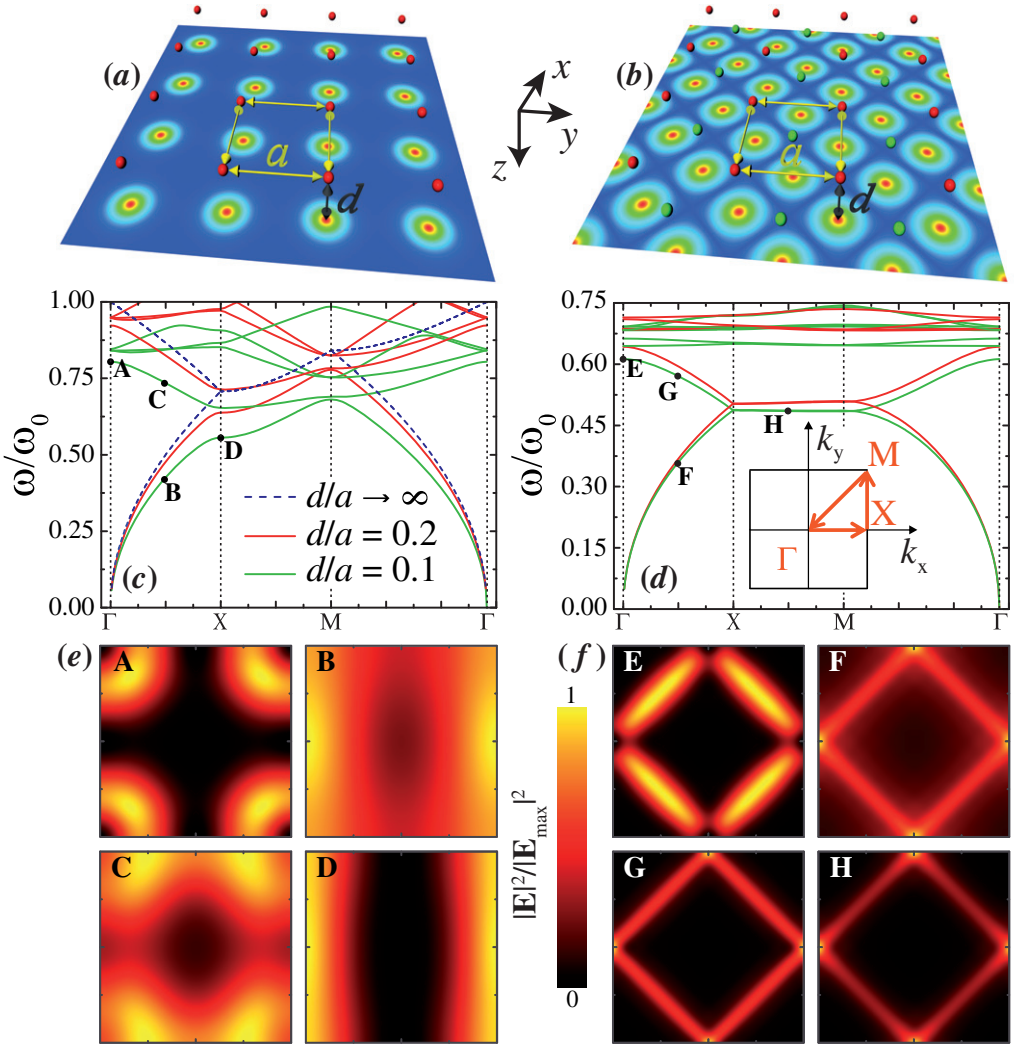

Figure 2. Plasmonic bands in periodically doped graphene. (a), (b) We consider two different doping configurations, produced by a square array of either (panels a, c, e) equal-sign point charges q (red dots in (a)) or (panels b, d, f) alternating-sign charges $(+q, -q, \ldots)$ (red and green dots in (b)). The lattice period a and the distance from the charges to the graphene d are shown in the upper schemes, along with density plots of the doping profiles $\langle|E_F|\rangle$. (c), (d) Plasmonic bands for different values of the d/a ratio, plotted along a representative excursion within the first Brillouin zone. The frequency ω is normalized to $\omega_0 = (e/\hbar)\sqrt{4\pi\langle|E_F|\rangle/a}$, where $\langle|E_F|\rangle$ is the average Fermi energy. (e), (f) Parallel-electric near-field intensities of representative plasmon modes over a unit cell at the graphene plane for $d/a = 0.1$, as indicated by labels A–H.

This allows us to scale all energies in our study by means of a characteristic frequency $\omega_0 = (e/\hbar)\sqrt{4\pi\langle|E_F|\rangle/a}$, where $\langle|E_F|\rangle$ is the average Fermi energy (see appendix A). The squared plasmon frequencies are directly proportional to the strength of the point charges, whereas the d/a ratio determines the amplitude of the periodic doping modulations. The simplicity of

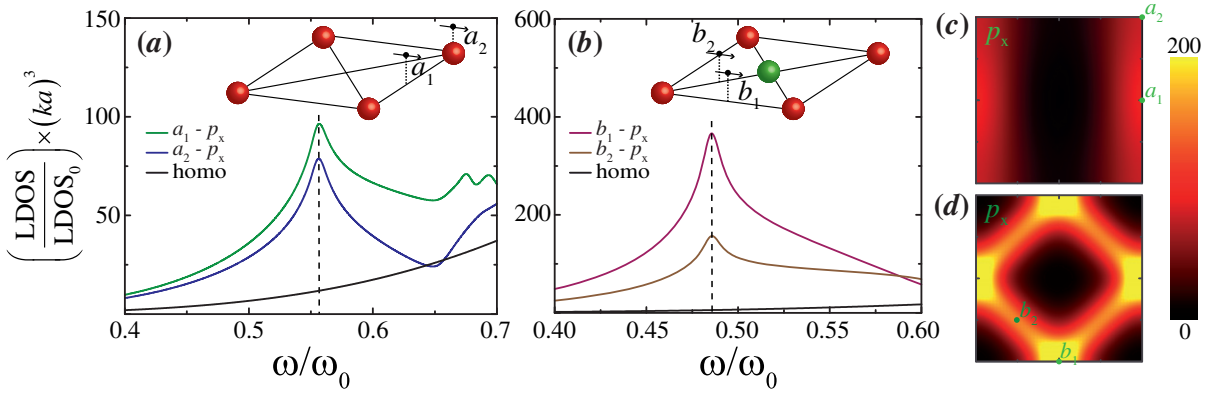

Figure 3. LDOS in periodically doped graphene. (a), (b) LDOS under the two configurations of figures 2(a) and (b) for $d/a = 0.1$. The orientation and different positions of the probing dipole are shown in the insets. (c), (d) In-plane dependence of the LDOS for the peak frequencies of panels (a) and (b), respectively (see dashed vertical lines). The LDOS is calculated at a distance $0.1a$ from the graphene plane in all cases.

this system allows us to obtain the plasmon bands and their contribution to the LDOS from a semi-analytical formalism, as described in detail in the appendix. All the presented calculations correspond to the choice $\gamma = 0.01\,\omega_0$, which is compatible with the low level of losses estimated for graphene plasmons from the measured high dc mobility [12, 26, 27].

The plasmon bands for equal-sign charges (figure 2(c)) evolve from those of homogeneous graphene in the $d \gg a$ limit (dashed curves) to develop substantial gaps in the X and M points for $d/a = 0.1$ (green curves). We show near-electric-field intensity distributions of selected modes in figure 2(e). Namely, A corresponds to a second-band mode of vanishing group velocity localized at the lattice sites; B represents a plasmon moving along the ΓX direction, with no significant modulations along ΓM; C is similar to B, but it shows one node along ΓM because it is in the second band and it has to be orthogonal to B; finally, D is also similar to B, but it exactly has a spatial period $2a$ along ΓX, and thus, its intensity shows maxima at every vertical row of lattice sites.

For alternating charge doping, the resulting band structure (figure 2(d)) displays a flat band that extends over a significant fraction of the first Brillouin zone (from X to M). The normalized frequency ω/ω_0 is rather independent of d/a, except for very small values of this ratio. Actually, both $\langle|E_F|\rangle$ and ω_0 are rapidly vanishing with increasing d/a as a result of sign cancellations in the doping potential (see the SI). In this limit, the doping charge exhibits a perfect harmonic profile with density $\approx(4q/a^2)\exp(-2\pi d/a)\,[\cos(2\pi x/a)+\cos(2\pi y/a)]$. The near-field intensities of selected modes (figures 2(e) and (f)) clearly show strong localization near the regions of vanishing doping charge (i.e. $\pm x \pm y = (n+1/2)a$, where n runs over integer numbers). This is similar to the trapping of plasmons at graphene p–n junctions [28], also predicted to occur at the center of ribbons under lateral gate doping [29]. We thus interpret the origin of the observed dispersionless bands in the strong localization of plasmons at the regions of vanishing doping charge. Interestingly, higher-order bands appear to be nearly dispersonless over the entire Brillouin zone.

Before discussing the explicit values of the LDOS offered in figure 3, it is interesting to explicitly point out that the decay rate of an emitter is simply given by $(4\pi^2\omega D^2/\hbar)\times$ LDOS,

where ω is the emission frequency and D is the transition dipole of the emitter. In free space, the LDOS projected along a given Cartesian direction reduces to $\mathrm{LDOS}_0 = \omega^2/3\pi^2c^3$. More details of the LDOS and its actual calculation are given in appendix B. Incidentally, the fraction of optical energy that is emitted as radiation is negligible near graphene [13], and it produces a contribution to the total decay rate that has a similar order of magnitude as the decay rate in vacuum, $4\omega^3 D^2/3\hbar c^3$.

Under doping with charges of equal sign, the first band has a saddle point where it crosses the X point and consequently, it is expected to produce a divergence in the LDOS [20], which is actually observed in figure 3(a). An even more pronounced singularity is associated with the first flat band in the XM region with alternating-sign doping charges (cf vertical scales of figures 3(a) and (b)). Compared with homogeneously doped graphene for the same level of average doping (i.e. the same $\langle|E_\mathrm{F}|\rangle$), we find a substantial enhancement of the decay rate by a factor of $\sim$8 in the same-sign array and $\sim$ 64 in the alternating-sign array. The dependence of the LDOS on the lateral position (figures 3(c) and (d)) fully confirms the symmetry of the bands contributing to the singularities: with equal-sign doping charges, the LDOS map (figure 3(c)) follows quite closely the near-field intensity at the singularity (i.e. near the saddle point D in figure 2(e)), which is dominated by field components along x, just like the probing dipole; also, for alternating-sign doping charges, the LDOS divergence extends over the entire region of vanishing doping, just like mode H in figure 2(f).

In summary, we have shown that periodically doped graphene exhibits Van Hove singularities in the plasmonic band structure that give rise to divergences in the LDOS. This is, in turn, translated into high values of the decay rate of optical emitters placed in the vicinity of the graphene. The emitted energy is almost entirely converted into plasmons, which are eventually dissipated as electron–hole pairs and heat. Interestingly, the transfer rate is boosted when we consider a doping profile that alternates sign along the carbon plane, as regions of vanishing doping produce dramatic localization of plasmon modes that contribute with relatively flat bands to the photonic structure, and therefore, even more pronounced singularities are obtained. The unprecedented levels of the LDOS observed with alternating-sign doped graphene structures could have practical relevance as a way to reach an ultrastrong light–matter interaction regime.

Acknowledgments

This work was partially supported by the European Union (FP7-ICT-2009-4-248855-N4E), the Spanish MEC (MAT2010-14885 and Consolider NanoLight.es) and Ibercivis. AM acknowledges financial support from the Spanish FPU.

Appendix A. Graphene plasmon bands

We consider a periodically doped graphene layer placed in the $z = 0$ plane. The period a is taken to be much smaller than the light wavelength, so that we can safely work in the electrostatic limit. Furthermore, we assume that the graphene responds locally with a conductivity $\sigma(\mathbf{R}, \omega)$ that depends on light frequency ω and position along the plane $\mathbf{R} = (x, y)$. We can directly write the total potential as the sum

$$\phi(\mathbf{r}, \omega) = \phi^{\mathrm{ext}}(\mathbf{r}, \omega) + \frac{\mathrm{i}}{\omega}\int \frac{\mathrm{d}^2\mathbf{R}'}{|\mathbf{r} - \mathbf{R}'|}\nabla'_\parallel \cdot \{\sigma(\mathbf{R}', \omega)[\nabla'_\parallel \phi(\mathbf{R}', \omega)]\}, \tag{A.1}$$

where $\phi^{\rm ext}$ is the external potential and we have defined $\nabla_\parallel = \hat{x}\frac{\partial}{\partial x} + \hat{y}\frac{\partial}{\partial y}$ and $\mathbf{r} = (\mathbf{R}, z)$. The integral term in equation (A.1) represents the contribution of the induced density, obtained from the continuity equation as $\rho = (-\mathrm{i}/\omega)\nabla_\parallel \cdot \mathbf{j}$, in which we express the induced current in terms of the parallel electric field as $\mathbf{j} = -\sigma\nabla_\parallel\phi$. An $\exp(-\mathrm{i}\omega t)$ time dependence is implicitly understood in these expressions.

We further assume the Drude model for the conductivity [12]

$$\sigma(\mathbf{R}, \omega) = \frac{\mathrm{e}^2}{\pi\hbar^2}\frac{\mathrm{i}|E_{\rm F}(\mathbf{R})|}{(\omega + \mathrm{i}\gamma)}, \tag{A.2}$$

where the damping rate γ satisfies $0 < \gamma \ll \omega$, and the Fermi energy depends on the local doping electron density $n(\mathbf{R})$ as $|E_{\rm F}(\mathbf{R})| = \hbar v_{\rm F}\sqrt{\pi|n(\mathbf{R})|}$. Clearly, the frequency dependence of σ comes through a multiplicative factor, and therefore, the periodicity of the structure allows us to write

$$\sigma(\mathbf{R}) = \sum_{\mathbf{G}} \sigma_{\mathbf{G}}\, \mathrm{e}^{\mathrm{i}\mathbf{G}\cdot\mathbf{R}}, \tag{A.3}$$

where the coefficients $\sigma_{\mathbf{G}}$ are independent of position. Likewise, we can expand the induced potential (i.e., the integral term in (A.1)) as

$$\phi^{\rm ind}(\mathbf{r}) = \sum_{\mathbf{G}} \phi^{\rm ind}_{\mathbf{G}}\, \mathrm{e}^{\mathrm{i}(\mathbf{G}+\mathbf{k}_\parallel)\cdot\mathbf{R} - |\mathbf{G}+\mathbf{k}_\parallel||z|}, \tag{A.4}$$

where the dependence on the parallel wave vector $\mathbf{k}_\parallel$ is inherited from the external potential. Inserting equations (A.3) and (A.4) into equation (A.1), and taking $z = 0$, we find

$$\phi_{\mathbf{G}} = \phi^{\rm ext}_{\mathbf{G}} + \sum_{\mathbf{G}'} \frac{(\mathbf{G}+\mathbf{k}_\parallel)\cdot(\mathbf{G}'+\mathbf{k}_\parallel)}{|\mathbf{G}+\mathbf{k}_\parallel|}\left(\frac{-2\pi\,\mathrm{i}\,\sigma_{\mathbf{G}-\mathbf{G}'}}{\omega}\right)\phi_{\mathbf{G}'}. \tag{A.5}$$

Before solving this equation, we work out the electron density under specific doping conditions.

We introduce the doping through a periodic array of external point charges placed at a distance d from the graphene. Considering first charges q of equal sign, we proceed by (i) using the method of images [30], (ii) expressing the Coulomb potential as

$$\frac{1}{r} = \int \frac{\mathrm{d}^2\mathbf{Q}}{(2\pi)^2}\frac{2\pi}{Q}\,\mathrm{e}^{\mathrm{i}\mathbf{Q}\cdot\mathbf{R} - Q|z|} \tag{A.6}$$

and (iii) performing the sum over charges via the identity

$$\sum_j \mathrm{e}^{\mathrm{i}\mathbf{Q}\cdot\mathbf{R}_j} = \frac{(2\pi)^2}{A}\sum_{\mathbf{G}}\delta(\mathbf{Q}-\mathbf{G}), \tag{A.7}$$

where A is the area of the unit cell and the sums run over 2D lattice sites $\mathbf{R}_j$ and reciprocal lattice vectors $\mathbf{G}$. We find that the screening electron density reduces to

$$n(\mathbf{R}) = \frac{q}{eA} f(\mathbf{R}), \tag{A.8}$$

where

$$f(\mathbf{R}) = \sum_{\mathbf{G}} \mathrm{e}^{\mathrm{i}\mathbf{G}\cdot\mathbf{R} - Gd} \tag{A.9}$$

and the 2D origin $R = 0$ is taken directly below one of the point charges. If we add an external point charge $-q$ at the center of each cell, we find instead

$$f(\mathbf{R}) = \sum_{\mathbf{G}} \mathrm{e}^{\mathrm{i}\mathbf{G}\cdot\mathbf{R} - Gd} \left\{1 - \cos[(G_x + G_y)a/2]\right\}. \tag{A.10}$$

Square lattices with both equal-sign and alternating-sign doping configurations are considered in this paper. Since $|E_\mathrm{F}|$ is proportional to $\sqrt{|n|}$, it is convenient to write the dimensionless function

$$g(\mathbf{R}) = \sqrt{|f(\mathbf{R})|} = \sum_{\mathbf{G}} g_{\mathbf{G}}\, \mathrm{e}^{\mathrm{i}\mathbf{G}\cdot\mathbf{R}}, \tag{A.11}$$

where we find the coefficients $g_\mathbf{G}$ from the above expressions for $f(\mathbf{R})$ through

$$g_{\mathbf{G}} = \frac{1}{A} \int_{\text{unit cell}} \mathrm{d}^2\mathbf{R}\, \mathrm{e}^{-\mathrm{i}\mathbf{G}\cdot\mathbf{R}} \sqrt{|f(\mathbf{R})|}. \tag{A.12}$$

From here, we can write the second fraction of equation (A.5) as

$$\frac{-2\pi \mathrm{i}\, \sigma_{\mathbf{G}}}{\omega} = \frac{a}{2\pi} \frac{\omega_0^2}{\omega(\omega + \mathrm{i}\gamma)} \frac{g_{\mathbf{G}}}{g_0}, \tag{A.13}$$

where

$$\omega_0 = \frac{e}{\hbar}\sqrt{4\pi \langle |E_\mathrm{F}| \rangle / a} \tag{A.14}$$

is a characteristic frequency of the system, expressed in terms of the average Fermi energy $\langle |E_\mathrm{F}| \rangle = g_0 E_\mathrm{F}^\infty$, where

$$E_\mathrm{F}^\infty = \hbar v_\mathrm{F} \sqrt{\pi |q|/eA} \tag{A.15}$$

is the Fermi energy obtained with equal-sign charges in the $d \gg a$ limit. The dependence of $g_0 = \langle |E_\mathrm{F}| \rangle / E_\mathrm{F}^\infty$ on d/a is shown in figure A.1 for both types of configurations.

A symmetric system of equations can be obtained by defining

$$\Psi_{\mathbf{G}} = \sqrt{|\mathbf{G} + \mathbf{k}_\parallel|}\, \phi_{\mathbf{G}} \tag{A.16}$$

in terms of which equation (A.5) reduces to

$$\Psi_{\mathbf{G}} = \Psi_{\mathbf{G}}^{\text{ext}} + \frac{\omega_0^2}{\omega(\omega + \mathrm{i}\gamma)} \sum_{\mathbf{G}'} N_{\mathbf{G},\mathbf{G}'}\, \Psi_{\mathbf{G}'}, \tag{A.17}$$

where we have used equation (A.13) and defined the dimensionless matrix

$$N_{\mathbf{G}\mathbf{G}'} = \frac{a}{2\pi} \frac{(\mathbf{G} + \mathbf{k}_\parallel) \cdot (\mathbf{G}' + \mathbf{k}_\parallel)}{\sqrt{|\mathbf{G} + \mathbf{k}_\parallel|\, |\mathbf{G}' + \mathbf{k}_\parallel|}} \frac{g_{\mathbf{G}-\mathbf{G}'}}{g_0}. \tag{A.18}$$

Finally, the plasmon bands are simply extracted from the real eigenvalues of this real-symmetric matrix λ_j as $\omega \approx \Omega_j - \mathrm{i}\gamma/2$, where

$$\Omega_j = \omega_0 \sqrt{\lambda_j}. \tag{A.19}$$

It is clear from equations (A.14) and (A.15) that the bands are directly tunable by changing the magnitude and distribution of the doping charges.

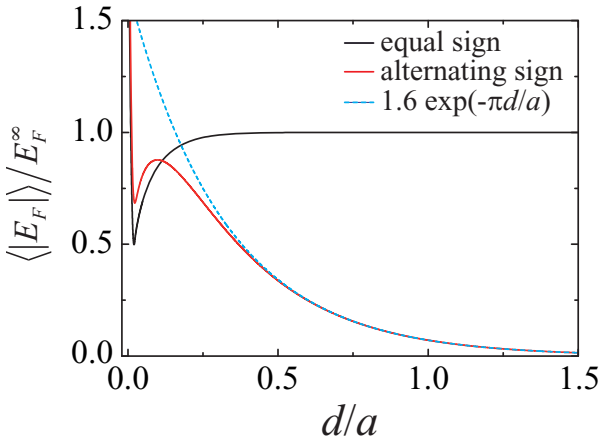

Figure A.1. Relation between the average Fermi energy $\langle|E_{\rm F}|\rangle$ and $E_{\rm F}^{\infty} = \hbar v_{\rm F}\sqrt{\pi|q|/eA}$ for square arrays of equal-sign and alternating-sign doping charges as a function of d/a. The asymptotic expression derived from the contribution of $(\pm1, 0)$ and $(0, \pm1)$ reciprocal lattice vectors in equation (A.10) is shown as a dashed curve.

Appendix B. Local density of optical states

The LDOS at a given position $\mathbf{r}_0$ can be obtained from the induced electric field $\mathbf{E}^{\rm ind}$ acting back on a dipole $\mathbf{p}$ placed at that position. More precisely [31], $\mathrm{LDOS} = \mathrm{LDOS}_0 + \mathrm{LDOS}_{\rm ind}$, where $\mathrm{LDOS}_0 = \omega^2/3\pi^2c^3$ is the value in vacuum projected along one of the three Cartesian directions, and

$$\mathrm{LDOS}_{\rm ind} = \frac{1}{2\pi^2\omega|p|^2}\mathrm{Im}\left\{\mathbf{E}^{\rm ind}(\mathbf{r}_0)\cdot\mathbf{p}^*\right\}. \tag{B.1}$$

We use equation (B.1) to obtain the LDOS in this paper, with the induced field calculated from the formalism of appendix A for the noted dipole source.

In our periodic configuration, using equation (A.6) and $\phi^{\rm ext}(\mathbf{r}) = -\mathbf{p}\cdot\nabla(1/|\mathbf{r}-\mathbf{r}_0|)$, it is convenient to write the external potential produced by the dipole at the graphene plane ($z = 0$) in parallel wave vector space as

$$\phi^{\rm ext}(\mathbf{R}, 0) = \sum_{\mathbf{G}}\int_{1\rm BZ}\frac{\mathrm{d}^2\mathbf{k}_\parallel}{(2\pi)^2}\mathrm{e}^{\mathrm{i}(\mathbf{G}+\mathbf{k}_\parallel)\cdot\mathbf{R}}\,\phi_{\mathbf{G}}^{\rm ext}, \tag{B.2}$$

where the $\mathbf{k}_\parallel$ integral is extended over the first Brillouin zone and

$$\phi_{\mathbf{G}}^{\rm ext} = -2\pi\left[\mathrm{i}\frac{(\mathbf{G}+\mathbf{k}_\parallel)}{|\mathbf{G}+\mathbf{k}_\parallel|}\cdot\mathbf{p} + \mathrm{sign}(z_0)\,p_z\right]\mathrm{e}^{-\mathrm{i}(\mathbf{G}+\mathbf{k}_\parallel)\cdot\mathbf{R}_0 - |\mathbf{G}+\mathbf{k}_\parallel||z_0|}. \tag{B.3}$$

Likewise, we can express the LDOS as an integral over $\mathbf{k}_\parallel$ components:

$$\mathrm{LDOS}_{\rm ind} = \int_{1\rm BZ}\mathrm{d}^2\mathbf{k}_\parallel\,\mathrm{LDOS}_{\rm ind}(\mathbf{k}_\parallel). \tag{B.4}$$

We solve each fixed $\mathbf{k}_\parallel$ component separately by expressing the self-consistent potential from equation (A.17) as

$$\begin{aligned}\Psi &= \left[1 - \frac{\omega_0^2}{\omega(\omega+\mathrm{i}\gamma)} N\right]^{-1} \Psi^{\mathrm{ext}} \\ &= \sum_j \left(\Psi_j^\dagger \cdot \Psi^{\mathrm{ext}}\right) \left[1 - \frac{\Omega_j^2}{\omega(\omega+\mathrm{i}\gamma)}\right]^{-1} \Psi_j, \end{aligned} \tag{B.5}$$

where N is given by equation (A.18) and the sum in the last line extends over orthonormalized eigenstates of this matrix (i.e. $N\Psi_j = \lambda_j \Psi_j$, such that $\Psi_j^\dagger \Psi_{j'} = \delta_{jj'}$ and $\sum_j \Psi_j \Psi_j^\dagger = \mathcal{I}$).

We obtain the induced field from the potential components (see equations (A.4) and (A.16)) as

$$\mathbf{E}^{\mathrm{ind}}(\mathbf{r}) = -\nabla\phi(\mathbf{r}) = -\nabla \sum_{\mathbf{G}} \int_{1\mathrm{BZ}} \frac{\mathrm{d}\mathbf{k}_\parallel}{(2\pi)^2} \mathrm{e}^{\mathrm{i}(\mathbf{G}+\mathbf{k}_\parallel)\cdot\mathbf{R} - |\mathbf{G}+\mathbf{k}_\parallel||z|} \phi_{\mathbf{G}}. \tag{B.6}$$

In this expression, which is used to compute electric near-field intensities, a dependence of $\phi_{\mathbf{G}}$ on $\mathbf{k}_\parallel$ is implicitly understood (see equations (A.4) and (A.5)). Inserting equation (B.6) into equation (B.1) and using equation (B.5), we find that

$$\mathrm{LDOS}_{\mathrm{ind}}(\mathbf{k}_\parallel) = \frac{1}{4\pi^3 \omega |p|^2} \sum_j \left|\Psi_j^\dagger \cdot \Psi^{\mathrm{ext}}\right|^2 \mathrm{Im}\left\{\frac{\Omega_j^2}{\Omega_j^2 - \omega(\omega+\mathrm{i}\gamma)}\right\}. \tag{B.7}$$

Finally, we calculate the LDOS from equations (B.4) and (B.7) by discretizing the first Brillouin zone and by choosing a small value of $\gamma = 0.01\omega_0$. Converged results are obtained for 200×200 points in $\mathbf{k}_\parallel$.

References

[1] Xu H, Bjerneld E J, Käll M and Börjesson L 1999 Spectroscopy of single hemoglobin molecules by surface enhanced raman scattering *Phys. Rev. Lett.* **83** 4357–60

[2] Atwater H A and Polman A 2010 Plasmonics for improved photovoltaic devices *Nature Mater.* **9** 205–13

[3] Danckwerts M and Novotny L 2007 Optical frequency mixing at coupled gold nanoparticles *Phys. Rev. Lett.* **98** 026104

[4] Kamat P V 2002 Photophysical, photochemical and photocatalytic aspects of metal nanoparticles *J. Phys. Chem.* B **106** 7729–44

[5] Purcell E M 1946 Spontaneous emission probabilities at radio frequencies *Phys. Rev.* **69** 681

[6] Frimmer M, Chen Y and Koenderink F A 2011 Scanning emitter lifetime imaging microscopy for spontaneous emission control *Phys. Rev. Lett.* **107** 123602

[7] Fussell D P, McPhedran R C and Martijn de Sterke C 2004 Three-dimensional Green's tensor, local density of states and spontaneous emission in finite two-dimensional photonic crystals composed of cylinders *Phys. Rev.* E **70** 066608

[8] García de Abajo F J and Kociak M 2008 Probing the photonic local density of states with electron energy loss spectroscopy *Phys. Rev. Lett.* **100** 106804

[9] Pockrand I, Brillante A and Möbius D 1980 Nonradiative decay of excited molecules near a metal surface *Chem. Phys. Lett.* **69** 499–504

[10] Blanco L A and García de Abajo F J 2004 Spontaneous light emission in complex nanostructures *Phys. Rev.* B **69** 205414

[11] Frimmer M and Koenderink F A 2012 Superemitters in hybrid photonic systems: a simple lumping rule for the local density of optical states and its breakdown at the unitary limit *Phys. Rev.* B **86** 235428
[12] Jablan M, Buljan H and Soljačić M 2009 Plasmonics in graphene at infrared frequencies *Phys. Rev.* B **80** 245435
[13] Koppens F H L, Chang D E and García de Abajo F J 2011 Graphene plasmonics: a platform for strong light–matter interactions *Nano Lett.* **11** 3370–7
[14] Wunsch B, Stauber T, Sols F and Guinea F 2006 Dynamical polarization of graphene at finite doping *New J. Phys.* **8** 318
[15] Chen J *et al* 2012 Optical nano-imaging of gate-tunable graphene plasmons *Nature* **487** 77–81
[16] Fei Z *et al* 2012 Gate-tuning of graphene plasmons revealed by infrared nano-imaging *Nature* **487** 82–5
[17] Thongrattanasiri S, Koppens F H L and García de Abajo F J 2012 Complete optical absorption in periodically patterned graphene *Phys. Rev. Lett.* **108** 047401
[18] Vakil A and Engheta N 2011 Transformation optics using graphene *Science* **332** 1291–4
[19] Manjavacas A, Thongrattanasiri S, Chang D E and García de Abajo F J 2012 Temporal quantum control with graphene *New J. Phys.* **14** 123020
[20] Van Hove L 1953 The occurrence of singularities in the elastic frequency distribution of a crystal *Phys. Rev.* **89** 1189–93
[21] Busch K and John S 1998 Photonic band gap formation in certain self-organizing systems *Phys. Rev.* E **58** 3896–908
[22] Bludov Yu V, Peres N M R and Vasilevskiy M I 2012 Graphene-based polaritonic crystal *Phys. Rev.* B **85** 245409
[23] Ferreira A and Peres N M R 2012 Complete light absorption in graphene-metamaterial corrugated structures *Phys. Rev.* B **86** 205401
[24] Peres N M R, Ferreira A, Bludov Y V and Vasilevskiy M I 2012 Light scattering by a medium with a spatially modulated optical conductivity: the case of graphene *J. Phys.: Condens. Matter* **24** 245303
[25] Song C-L, Sun B, Wang Y-L, Jiang Y-P, Wang L, He K, Chen X, Zhang P, Ma X-C and Xue Q-K 2012 Charge-transfer-induced cesium superlattices on graphene *Phys. Rev. Lett.* **108** 156803
[26] Novoselov K S, Geim A K, Morozov S V, Jiang D, Zhang Y, Dubonos S V, Grigorieva I V and Firsov A A 2004 Electric field effect in atomically thin carbon films *Science* **306** 666–9
[27] Novoselov K S, Geim A K, Morozov S V, Jiang D, Katsnelson M I, Grigorieva I V, Dubonos S V and Firsov A A 2005 Two-dimensional gas of massless Dirac fermions in graphene *Nature* **438** 197–200
[28] Mishchenko E G, Shytov A V and Silvestrov P G 2010 Guided plasmons in graphene p–n junctions *Phys. Rev. Lett.* **104** 156806
[29] Thongrattanasiri S, Silveiro I and García de Abajo F J 2012 Plasmons in electrostatically doped graphene *Appl. Phys. Lett.* **100** 201105
[30] Jackson J D 1999 *Classical Electrodynamics* (New York: Wiley)
[31] Novotny L and Hecht B 2006 *Principles of Nano-Optics* (New York: Cambridge University Press)